Conjugate Jet Impingement Heat Transfer Investigation via Transient Thermography Method

Beni Cukurel*
Technion — Israel Institute Technology, Technion City, 32000 Haifa, Israel
Matthieu Fénot†
Université de Poitiers, 86961 Chasseneuil, France
and
Tony Arts‡
Von Karman Institute for Fluid Dynamics, 1640 Rhode-St-Genèse, Belgium

DOI: 10.2514/1.T4462

Investigating the conduction–convection coupling, the present study is focused upon measurement of conjugate heat transfer ensuing jet impingement on a 15-mm-thick metallic plate. Based on a rapid change in jet temperature and using time-accurate infrared thermography, a transient measurement methodology is developed toward acquisition of heat transfer coefficients. The new technique is shown to have comparable levels of Nusselt number and effectiveness accuracy, all while significantly reducing the number of consecutive measurements and their duration. To highlight the significance of the conjugate effect, different plate materials (copper, steel, and Inconel) are employed to differ the solid thermal conductivities, resulting in Biot-number variations. The plate surface heat transfer is studied at two injection Reynolds numbers (34,000 and 37,000) and for two nozzle-to-plate distances (two and five jet diameters). The changes in slab material conductivity reveal small but quantifiable differences in heat transfer coefficients (up to ∼20% locally and 9% globally). Furthermore, constituting an upper bound and lower bound, respectively, it is observed that all conjugate Nusselt number distributions lay within the two limits of isoheat flux and isothermal boundary condition cases.

Nomenclature

Bi	=	$he/\lambda_{\text{solid}}$, Biot number
Br	=	$(e/x)K^{-1}(Pe)^{1/3}$, Brun number
C	=	heat capacity, $\text{J} \cdot \text{kg}^{-1} \cdot \text{K}^{-1}$
D	=	jet diameter, m
E	=	impingement plate thickness, m
H	=	heat transfer coefficient on the impinging side, $\text{W} \cdot \text{m}^{-2} \cdot \text{K}^{-1}$
H	=	jet exit to impingement plate distance, m
h_{lat}	=	heat transfer coefficient on the lateral side of the slab, $\text{W} \cdot \text{m}^{-2} \cdot \text{K}^{-1}$
K	=	$\lambda_{\text{solid}}//\lambda_{\text{air}}$
Nu	=	hD/λ_{air}, Nusselt number
Nu_0	=	Nusselt number at the impingement point
Pe	=	$Pr \times Re$, Peclet number
Pe^*	=	conjugate Peclet number, $K^{-1} \cdot Pe^{1/3}$
Pr	=	Prandtl number
R	=	impingement plate radius, m
Re	=	$\rho VD/\mu$, jet Reynolds number
r	=	radial coordinate, m
T_{aw}	=	adiabatic wall temperature, K
T_j	=	injection jet temperature, K
T_{ref}	=	T_{aw}, reference temperature in Newton's law of cooling, K
T_w	=	impinging side wall temperature, K
T_{w0}	=	impinging point wall temperature, K
T_∞	=	ambient temperature, K
V_j	=	injection velocity, $\text{m} \cdot \text{s}^{-1}$
ε_w	=	impinging side emissivity
η	=	$(T_{\text{ref}} - T_\infty)/(T_j - T_\infty)$, effectiveness
θ	=	$(T_w - T_\infty)/(T_{w0} - T_\infty)$
λ	=	thermal conductivity, $\text{W} \cdot \text{m}^{-1} \cdot \text{K}^{-1}$
μ_{air}	=	air dynamic viscosity, $\text{N} \cdot \text{s} \cdot \text{m}^{-2}$
ρ	=	density, $\text{kg} \cdot \text{m}^{-3}$
φ_{co}	=	convective heat-flux density of the impingement plate, $\text{W} \cdot \text{m}^{-2}$
φ_{elec}	=	electrical flux density dissipated by Joule effect, $\text{W} \cdot \text{m}^{-2}$

Received 18 April 2014; revision received 15 January 2015; accepted for publication 18 February 2015; published online 30 June 2015.

*Lecturer, Faculty of Aerospace Engineering.
†Assistant Professor, Département Fluides, Thermique, Combustion; Institut P', CNRS-ENSMA, 1 Avenue Clément Ader.
‡Professor, Turbomachinery and Propulsion Department, UPR 3346, BP 40109.

I. Introduction

JET impingement can provide high rates of heat transfer in a wide range of applications, and as such it has been extensively investigated both experimentally and numerically. Focusing on the aerodynamic flow structure and the associated convective heat transfer, wide-ranging literature surveys on the topic demonstrated the effects of Reynolds number, nozzle-to-plate distance, nozzle geometry, jet temperature, jet orientation, multiple jets, crossflow, and impingement surface shape [1–3]. Nevertheless, most of the jet impingement studies in prior literature are purely convective and therefore involve artificial thermal boundary conditions imposed at the solid–fluid interface: in general, a Neumann boundary condition [4,5] or a Dirichlet boundary condition [6]. In applications with highly coupled interface heat flux and temperature, this modeling approach may not be sufficiently accurate. In comparison, for the conjugate heat transfer case, the effects of the solid domain conduction are coupled with the convection over the surface (i.e., the thermal history of the boundary layer is accurately modeled). Hence, no constraint is enforced at the solid–fluid interface, except for thermal equilibrium and heat-flux continuity. The methodology of conjugate heat transfer analysis presents the opportunity to accurately model the true heat transfer mechanisms.

II. Fundamental Background

The goal of this paper is to present a new methodology that is applicable to conjugate heat transfer investigations and to

demonstrate its ramifications on a sample study conducted in jet impingement configuration.

From a wide range of experimental measurement techniques commonly found in convective heat transfer literature, few are applicable to conjugate cases. Among steady-state techniques, it is evident that the lengthy testing period of several hours associated with establishing equilibrium for each data point raises issues with maintaining aerothermal boundary conditions. Addressing this complication, prior literature on the subject presents a hybrid transient step heating measurement technique for a mostly uniform interface heat-flux boundary condition, which is further refined by lateral conduction loss corrections [7]. However, due to the prescribed interface flux requirement, this methodology is not directly applicable to the conjugate problem. Therefore, a new transient measurement methodology, which is inherently tailored toward conduction coupled convective heat transfer problems, is presented and validated.

The present research effort is devoted to a deeper understanding of the conjugate heat transfer phenomenon in jet impingement geometries. Because of the scarcity of conjugate data (especially experimental), this contribution could serve as a baseline for future efforts. Contrasting the jet impingement heat transfer coefficients associated with different solid thermal conductivities, the presented work exemplifies the experimental efforts to include the effects of conduction coupling in forced convection applications.

A. Similarity Analysis

Considering flow over a fixed geometry, where a coupled convection–conduction heat transfer phenomenon takes place, the dimensionless Buckingham π parameters can be expressed as

$$f(Re, Pr, Ec, T_\infty/\Delta T, Nu, K, Bi) = 0 \tag{1}$$

where Ec, $T_\infty/\Delta T$, Nu, K, and Bi are the Eckert number, the scaled relative bulk flow temperature, the Nusselt number, the solid–fluid thermal conductivity ratio, and the Biot number. In the present configuration, the physical properties of the fluid do not vary significantly (limited variations of $T_\infty/\Delta T$ and Pr), and the relative importance of the kinetic energy with respect to the enthalpy is small (limited variation of Eckert number). Hence, it can be inferred that

$$Nu = f(Re, K, Bi) \tag{2}$$

Thus, for a conjugate problem with fixed geometrical and aerodynamic constraints, the heat transfer depends not only on the local flow but also on the solid and air thermal conductivities, as well as on the thickness of the material. The intensity of the conjugate heat transfer effect is in part determined by the solid-to-fluid thermal conductivity ratio K. In the case of a given wall-to-fluid temperature head $(T_w - T_\infty)$ variation, this ratio largely specifies the heat transfer distribution driven by the nonisothermal character of the surface. In turn, the Biot number incorporates the flux reallocation effects, and it is therefore typically used as a criterion to estimate the extent of the coupling. There can be alternative formulations that characterize the body–fluid thermal resistances: the Brun number [8], which gives a measure of the thermal resistance of the plate to that of the laminar boundary layer, and the conjugate Peclet number [9], which is the ratio of the rate of advection by the flow to the rate of diffusion:

$$Br = (e/L)K^{-1}Pe^{1/3} \tag{3}$$

$$Pe^* = K^{-1}Pe^{1/3} \tag{4}$$

The conjugate heat transfer problem considers the thermal interaction between a body and a fluid flowing over it, as a result of which a particular temperature distribution is established on the interface. Hence, from the perspective of the fluid, the properties of heat transfer of any conjugate problem are identical to those of its convective counterpart, as long as an identical nonuniform temperature field can be imposed along the wetted surface. Thus, in general, the theory of conjugate heat transfer is in fact the theory of flow over an arbitrarily nonisothermal surface, where the interface temperature distribution is unknown a priori.

B. Conjugate Heat Transfer

In convection problems, the generally unknown temperature and heat-flux distributions at the solid–fluid interface was coined by Perelman [10] as conjugated heat transfer. Fundamental analytical studies of the laminar flow over a heated flat plate were carried out by Dorfman [11,12]. The findings highlighted the role of the streamwise temperature gradients on the local heat transfer; whereas increasing the temperature head resulted in augmented heat transfer coefficients, the contrary case of decreasing the temperature head led to a lower than isothermal boundary condition heat transfer [12–14]. In similar numerical studies on laminar flow inside a circular tube [15,16], when the interface boundary condition was switched from isoheat flux (convective) to conjugate, the results indicated a global Nusselt number reduction of up to 10% [16].

Studying the incompressible laminar fluid flow along a flat plate that was uniformly heated at the backside, the literature highlighted the conjugate heat transfer dependence on the thermal conductivity ratio [17,18]. Simplified expressions for the calculation of surface temperature, heat flux, and Nusselt number reduced the dependency to a function of the Brun number [19]: for values higher than 0.1, the selection of boundary condition (conjugate or isothermal) altered the heat transfer by more than 5% [19].

Several authors tried to decouple the heat transfer coefficient from the wall boundary conditions. In a channel flow with six separate surface temperature distributions, referencing the fluid inlet temperature, the resultant heat transfer coefficients led to discrepancies up to 24%, whereas the adiabatic wall temperature definition reduced the coefficient variance to within 5% [20]. Similarly, for laminar flow inside a duct with Biot number greater than 1, a decoupling interface between independent conduction and convection solvers was achieved by using the adiabatic wall temperature as the fluid reference temperature [21].

Although analyzing heat transfer problems from a conjugate perspective has gained attention recently, the literature on conjugate jet impingement heat transfer remains limited. The time-dependent impingement of a free, high-Prandtl-number, fluid jet on a solid disk of finite thickness was numerically evaluated [22]. In the simulation, it was confirmed that, in addition to the jet Reynolds number, the plate thickness and its thermal conductivity have a significant impact on the local temperature distribution and the associated heat transfer. In a more fundamental investigation, an arbitrary temperature and heat flux was prescribed on the nonwetted surface of a plate subjected to laminar jet impingement [23,24]. The local heat transfer coefficient was influenced by the Prandtl number, the ratio of fluid to solid conductivities and the disk thickness. For thin disks, the study highlighted that the distribution of the imposed back side boundary condition had a significant effect.

Toward expanding the scientific knowledgebase in conjugate jet impingement heat transfer, this research effort experimentally investigates the ramifications of solid conduction variation on jet impingement heat transfer via a new transient measurement methodology.

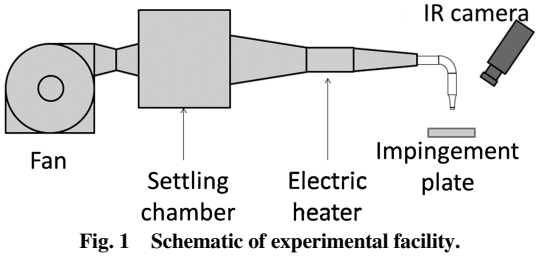

Fig. 1 Schematic of experimental facility.

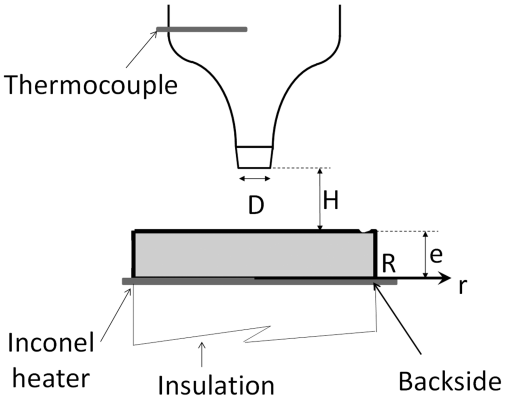

Fig. 2 Test section.

III. Experimental Setup

A. Jet Impingement Facility

The experiment is conducted with a round air jet from a contraction nozzle at two injection Reynolds numbers ($Re = 34,000$, 37,000), impinging on a flat plate at two nozzle-to-plate distances ($H/D = 2$, 5) and for three slab materials (copper, steel, and Inconel). A schematic of the experimental facility is presented in Fig. 1, and a detailed view of the test section is shown in Fig. 2.

The airflow, generated by the blower, is guided through a settling chamber, which damps the supply pressure fluctuations. The air is then passed through a convergent section and ducted into an electrical heat exchanger. Based on prior designs presented in literature [25,26], the circuit is composed of six metallic meshes connected in series to a 50 V 60 A dc power supply. Depending upon the supplied current, a rapid flow temperature change (in the order of 35 K) is obtained within 3 s. Finally, the flow is channeled through a thermally insulated axisymmetric convergent injection nozzle (Fig. 2). Reducing the mean flow nonuniformities, the 40-mm-long contraction is designed with an area ratio of 23 and produces a flat velocity profile at the 8-mm-diam exit. The mean jet velocity and temperature are characterized by total pressure and thermocouple measurements upstream of the nozzle.

The prescribed flow impinges upon a cylindrical slab of radius $R = 54$ mm ($6.75D$) and of thickness $e = 15$ mm made of copper, steel, or Inconel; their thermal properties are summarized in Table 1. Analyzing the conjugate Peclet numbers, and considering the trends observed in [27], it is expected that, as Pe^* rises, the deviation from the adiabatic-case heat transfer coefficient increases. Alternatively, with the local Brun number (Br) estimation of 0.085 and 0.14 for steel and Inconel, respectively, the conduction–convection coupling effects are deemed nonnegligible [19].

The investigations are conducted in the heating mode of the conjugate interaction (i.e., the impingement plate temperature is higher than the jet temperature). Thereby, a higher surface flux level can be achieved, reducing the experimental error. To provide constant heat flux to the backside of the slab, a 25-μm-thick Inconel foil, with a resistance of $0.063 \pm 0.005\Omega$, is heated via the Joule effect. The uniform heat flux density imposed on the backside surface was verified in a previous investigation [28]. The slab and heater assembly is placed on a 40-cm-thick insulation, and the heat flux losses into the insulation are estimated to be of the 0.7% order.

The temperature distribution created at the solid–fluid boundary of the slab is measured by the 14-bit FLIR SC 3000 infrared camera, located above the test section at 30 deg from the vertical axis. The top surface of the slab is coated with Nextel black paint to ensure high and uniform emissivity for infrared thermography measurements ($\varepsilon_w = 0.95$). The thickness of the paint layer is 100 μm, and its thermal properties are $\lambda_p = 0.14 \pm 0.015$ W $\cdot$ m^{-1} $\cdot$ K^{-1}, $\rho_p = 1650 \pm 20$ kg $\cdot$ m^{-3}, $C_p = 550 \pm 20$ J $\cdot$ kg^{-1} $\cdot$ K^{-1}. The perspective distortions of the acquired image are corrected using a bicubic interpolation scheme. Considering the axisymmetric character of the problem, the temperature distributions are averaged in the azimuthal direction, resulting in a single curve in the radial direction at each time instant.

B. Conjugate Heat Transfer Measurement Methodology

In conjugate heat transfer experiments, there is no artificial constraint imposed on the solid–fluid interface; the wetted surface boundary condition is altered by varying the heat flux values on the backside of the plate and through their conduction driven redistribution. However, although the surface temperature (T_w) is measured directly by infrared thermography, the convective heat-flux density φ_{co} can only be numerically computed by solving the solid conduction. Because of the axisymmetric jet flow and the circular geometry of the slab, a two-dimensional computational domain is implemented in COMSOL Multiphysics (Fig. 3). A radial cross section of the plate, including the paint layer, is modeled with an unstructured mesh consisting of 150,000 triangular elements. Based on the one-dimensional unsteady heat transfer equation, and toward maintaining a relatively uniform Courant number across the two solid regions, the element length sizes of the metallic slab and the paint layer are scaled by the square root of their thermal diffusivities. Further mesh refinements do not alter the local temperature distributions.

The boundary conditions of the computational domain are the imposed uniform electrical heat-flux density at the bottom (φ_{elec}), the infrared measured wall temperature distribution on the top (T_w), a symmetry boundary condition at the centerline, and a constant uniform heat transfer coefficient on the lateral surface, $h_{\text{lat}} = 10$ W/m^2 $\cdot$ K. The resultant model enables computation of the wetted surface convective heat-flux density φ_{co}.

1. *Steady-State Technique*

The multiflux steady-state measurement technique is well established in the heat transfer literature and has been previously employed in various purely convective studies [5,29]. The method is based on the general definition of the heat transfer coefficient, based on Newton's law:

$$T_w = \frac{\varphi_{\text{co}}}{h} + T_{\text{ref}} \tag{5}$$

For a given combination of a Reynolds number and a nozzle-to-plate distance, the technique consists of imposing different flux values on the heater, which result in altered steady-state wetted boundary conditions. At each thermal equilibrium point, the ensuing wall temperature T_w (average of 40 thermographic images recorded over 10 s) is experimentally measured, and the convective heat-flux density φ_{co} is numerically evaluated. Repeating this procedure for four different electrical heat-flux densities φ_{elec}, the convective heat transfer coefficient h and the reference temperature T_{ref} are obtained using linear regression. In this case, the reference temperature T_{ref} corresponds to the adiabatic wall temperature T_{aw}, the temperature observed at the wall when the heat-flux density is equal to zero. The results are presented in their nondimensional form:

Table 1 Thermal properties and conjugate heat transfer criteria of plate materials

Material	λ, W $\cdot$ m^{-1} $\cdot$ K^{-1}	ρ, kg $\cdot$ m^{-3}	C, J $\cdot$ kg^{-1} $\cdot$ K^{-1}	K	Pe^*	Br
Copper	400 ± 20	8960 ± 115	380 ± 15	~14000	~0.002	~0.004
Steel	18.6 ± 1	7966 ± 100	540 ± 20	~650	~0.045	~0.085
Inconel 600	11.6 ± 0.5	8440 ± 110	448 ± 17	~400	~0.074	~0.140

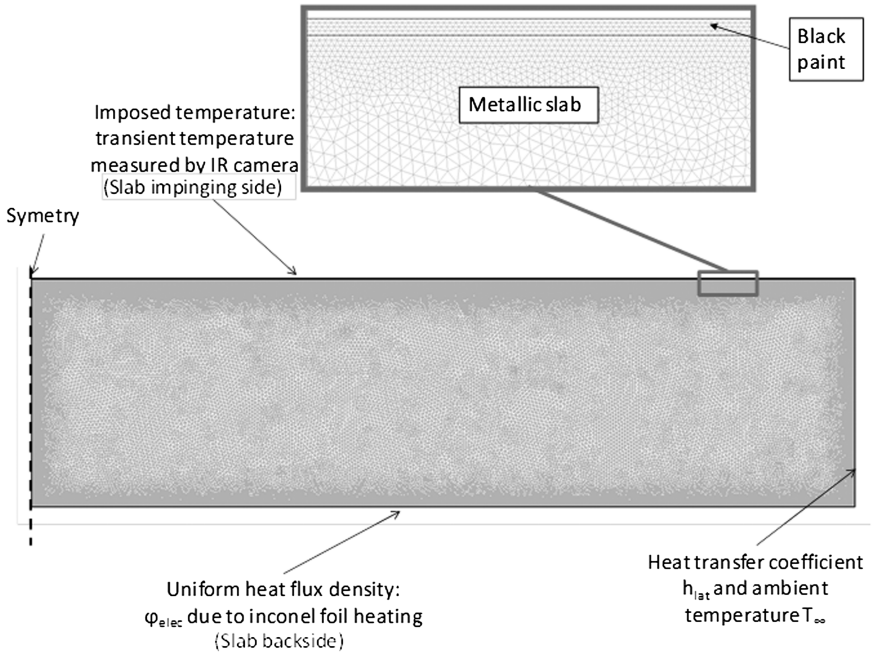

Fig. 3 Computational domain with boundary conditions.

$$Nu = \frac{hD}{\lambda_{\text{air}}} \tag{6}$$

$$\eta = \frac{T_{\text{aw}} - T_\infty}{T_j - T_\infty} \tag{7}$$

where the air thermal conductivity λ_{air} is calculated using the adiabatic wall temperature. Prior investigations on the subject demonstrated that the resulting Nusselt number Nu and effectiveness η are independent of $T_j - T_\infty$ and therefore adequately characterize the solution set [5,30]. However, due to conduction thermal equilibrium time scales, the application of the multiflux steady-state technique is cumbersome because achieving solid thermal equilibrium for all four distinct heat-flux values requires 5 h of experimentation time at each aerodynamic condition (distinct h, η).

2. Transient Change Technique

In contrast, the transient change technique is aimed to eliminate the necessity to reach steady state at several flux operating conditions. Because the Nusselt number and the effectiveness are independent of the jet temperature T_j, Eq. (5) can be rewritten in terms of the nondimensional parameters [Eqs. (6) and (7)]:

$$\varphi_{\text{co}} = \frac{\lambda_{\text{air}} Nu}{D}[T_w - (\eta(T_j - T_\infty) + T_\infty)] \tag{8}$$

Therefore, at constant aerodynamic boundary conditions (ambient temperature T_∞, jet Reynolds number Re) and for a given electrical heat-flux density φ_{elec}, Nu and η can be determined by changing the jet temperature T_j. By evaluating Eq. (8) at each time instance, a set of equations is formed. With the recorded time variant wall temperature distribution T_w, as well as the numerically evaluated unsteady surface heat flux φ_{co}, the overdetermined system of equations is solved for the best fitting values of Nu and η.

Initially, to prescribe an initial known surface flux condition $\varphi_{\text{co}}(r, 0)$ to the numerical unsteady conduction model, the slab is brought to thermal equilibrium for a fixed φ_{elec} and a jet temperature equal to that of the ambient, $T_j(0) = T_\infty$. Consequently, a rapid change of the jet temperature $T_j(t)$ is prescribed and recorded, and all the while, the resulting wall temperature time evolution $T_w(r, t)$ is captured by the infrared camera. The image acquisition frequency is kept at 4 Hz because higher sampling rates (up to 50 Hz) did not present any improvements in measurement accuracy. The temporal convective surface heat flux $\varphi_{\text{co}}(r, t)$ is then computed by solving the unsteady conduction equation in the slab. Consequently, by evaluating $\varphi_{\text{co}}(r, t)$ and $T_w(r, t)$ in Eq. (8), the independent variables Nu and η are estimated using the method of least squares.

Contrasting the procedure steps for steady-state and transient measurements, Fig. 4 summarizes the detailed experimental procedure for both techniques. Using the transient technique, it was observed that the testing time was reduced to the time required for the thermal equilibrium of a single aerothermal boundary condition. Therefore, the transient methodology is five times faster than the multiflux steady-state technique.

C. Uncertainty Analysis

The suggested method for heat transfer coefficient h measurement suffers from three uncertainty sources originating from the contributions of the wall temperature, the COMSOL calculated surface heat flux, and the freestream air temperature. The measurement error is quantified within a 95% confidence interval, acquired by the single sample uncertainty analysis proposed in [31].

The overall uncertainty associated with the wall temperature measurements can be decomposed into several contributing factors, including the uncertainty associated with the calibration of the thermocouples, the variation of the object signal due to camera noise, and the uncertainty introduced by the infrared image processing, as well as filtering and curve fitting. The calibration of the T-type thermocouples is conducted in a temperature-controlled oil bath by means of a thermometer with a resolution of 0.1 K. Including the effects of the analog-to-digital discretization error, the thermocouple data uncertainty is computed to be 0.18 K. The infrared camera object signal, as function of the spatial location and the surface temperature, varies on average by 3.2 intensity units among 40 consecutive images. Considering the calibration curve slope, the uncertainty of the temperature measured by the infrared camera was 0.06 K. It was experimentally observed that the surrounding reflections can contribute to bias errors of the object signal, which correspond to temperature deviations of up to 0.2 K. Another uncertainty factor is the azimuthal direction temperature nonuniformity at a given camera calibration instance, which is calculated to be in the order of 0.1 K. The uncertainty contribution of the filtering procedure to the raw infrared images is around 0.15 K. Last, the uncertainty introduced by the calibration curve fitting procedure is quantified as the deviation of the points from the second-order polynomial fit (up to 0.12 K). Considering the aforementioned quantities, the cumulative infrared

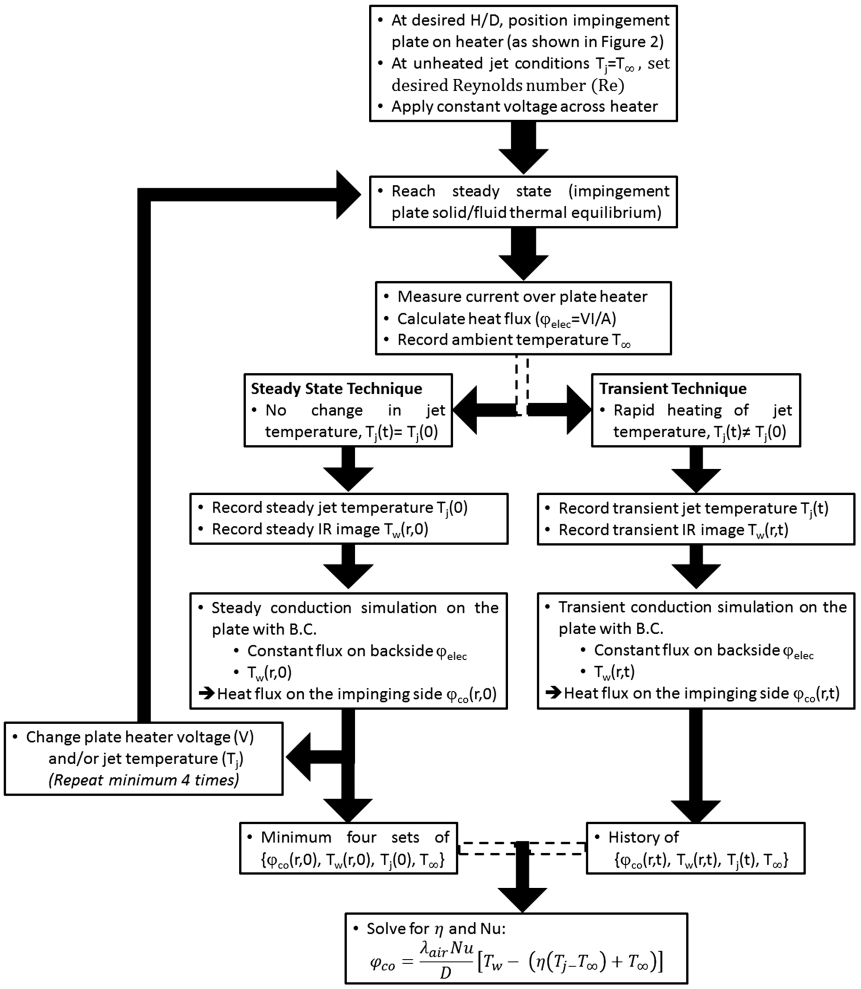

Fig. 4 Flowchart description of steady-state and transient measurement techniques.

thermography wall temperature measurement accuracy is estimated to be ±0.35 K within a 95% confidence interval.

The local jet temperature T_∞ is computed from the thermocouples located upstream of the injection nozzle. The resulting cumulative jet air temperature uncertainty is estimated to be in the order of 0.55 K.

The numerical computation of heat flux at the wetted surface of the slab was performed using data from the experiment to set the boundary conditions, specifically, the measured wall temperature on the wetted side and the heat flux imposed on the backside of the slab. Looking at experimental uncertainty propagation into numerical models, Rabin [32] considers a deterministic perturbation approach to each of the physical independent quantities; the differences with the unperturbed solution provide an estimate on sensitivities. Perturbations in the backside boundary heat-flux and wall temperature measurement uncertainty, along with error in paint and slab properties, are observed to propagate and produce a nonuniform surface heat-flux uncertainty.

The typical distribution of the uncertainty estimations of Nusselt number Nu and effectiveness η) along the plate radius are presented in Fig. 5 for both steady and transient methodologies. In general, the uncertainties associated with the two methods are of the same magnitude. The steady-state method is slightly more accurate; this is predominantly associated with the limited knowledge of paint and slab diffusivities (ρ and C) needed in the transient calculations. Nevertheless, it is important to note that the shortcomings of the steady-state technique associated with jet and ambient temperature variations (temporal nonuniformity due to the difficulty in maintaining test conditions) are not taken into account.

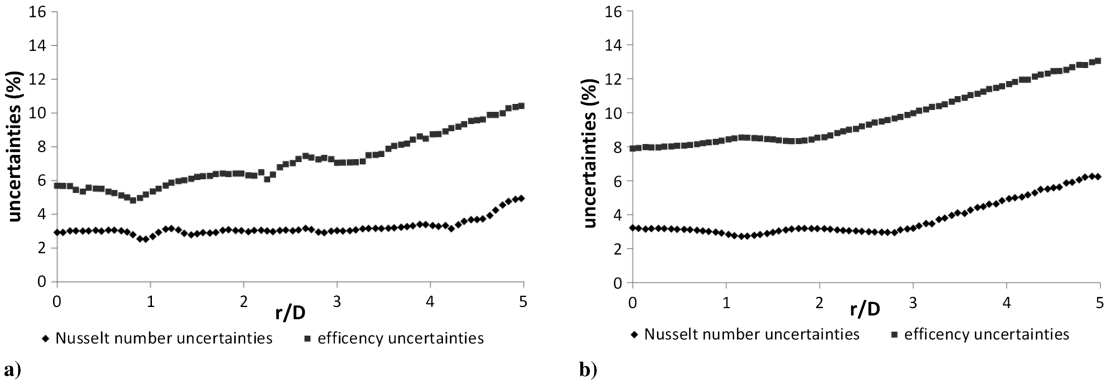

Fig. 5 Typical uncertainty distribution for a) steady-state method, and b) transient method.

IV. Results and Discussion

A. Transient Method Validation

To verify the transient conjugate heat transfer measurement technique, exemplary results are compared with those obtained from the conventional multiflux steady-state methodology, which is typically employed in convective investigations. For the baseline geometrical configuration ($Re = 34,000$, $H/D = 5$) the Nusselt number and effectiveness along the steel slab are presented in Figs. 6 and 7. The charts compare the local distributions of heat transfer coefficient and effectiveness, computed using the steady reference technique, as well as the transient jet temperature change method.

To demonstrate the robustness of the transient methodology, three independent parametric tests are conducted for different combinations of jet temperature variation ΔT_j and backside heat-flux values φ_{elec}. For imposed boundary conditions of ($\varphi_{\text{elec}} =$ 18 kW, $\Delta T_j = 40$ K), ($\varphi_{\text{elec}} = 18$ kW, $\Delta T_j = 30$ K), and ($\varphi_{\text{elec}} =$ 15 kW, $\Delta T_j = 40$ K), the general distributions of Nusselt number indicate negligible deviations amongst all cases (Fig. 6). Although slight effectiveness variations exist in the vicinity of the impingement point (Fig. 7), the differences diminish at greater radial distances ($r/D > 2.2$). It is noteworthy that, for all three sets of boundary conditions, the discrepancies in Nu and η are lower than the respective uncertainties. Hence, the heat transfer quantities, measured using the transient method, are observed to be independent of the electrical heat-flux density, the magnitude of the change in jet temperature, as well as the jet injection temperature T_j.

Having determined the precision of the transient technique, the accuracy of the findings is compared with the results obtained from the multiflux method. In Fig. 6, the locations of local minima and maxima in the radial Nusselt number distributions are seen to coincide for both methods. The effectiveness curves present similar general trends, despite deviations of the uncertainty order at greater radial distances $r/D > 4$ (Fig. 7). This slight discrepancy is believed to be predominantly associated with the multiflux technique; because it assumes constant ambient temperature throughout the entire duration of the experiment, and considering the extensive testing periods (5 h), which can result in shifts of T_∞, the conventional steady-state method is inferred to be inherently more prone to errors. Nevertheless, the Nusselt number and effectiveness distributions, acquired by the multiflux and transient techniques, show good agreement and fall within the range of values set out in previous investigations [3,33]. Because the steady-state technique is time-consuming (5 h) and suffers from issues associated with maintaining the external boundary conditions (such as the surrounding air temperature), the transient technique is used throughout the remaining part of the study.

B. Jet Impingement Heat Transfer

In general, the jet impingement flowfield is divided into three regions: a free jet characterized by the potential jet core surrounded by a shear layer, a stagnation area where the jet flow turns radially outward while the shear-layer vortices are deflected and roll along the impinging plate, and a wall jet zone in which the plate parallel flow develops the boundary layer. Characteristic jet impingement heat transfer is associated with significantly augmented values around the stagnation point and a gradual reduction trend at increased radial distances. The first maximum is usually close to the impingement point ($r/D < 0.5$); however, the local peak is not as prevalent in all studies [4,29]. Furthermore, for low nozzle-to-plate distances and high injection Reynolds numbers, the heat transfer distribution in the radial direction exhibits a secondary peak.

With the validated transient methodology, the conjugate jet impingement heat transfer over the Inconel slab is analyzed at two injection distances ($H/D = 2$ and 5), for which Figs. 8 and 9 present the Nusselt number Nu and the effectiveness η distributions, respectively. For a small jet-to-plate spacing ($H/D = 2$), the Nusselt number shows a local minimum at the impinging point, followed by a maximum at r/D equal to 0.3. This phenomenon has been previously observed in impingement geometries with convergent injection nozzles [34–36]. The established explanation is associated with a flat jet injection velocity profile, for which the turbulence intensity attains a maximum at $r/D = 0.2$ to 0.5 due to the shear-layer impingement [36]. On the contrary, for a fully developed flow injection profile resulting from a tubular $20D$ pipe nozzle, the velocity distribution has its maximum close to the jet axis, and the consequent heat transfer maximum is situated at the impingement point [36]. At greater radial distances, Fig. 8 shows the presence of a second global maximum at $r/D = 1.6$. The relevant literature associated with small nozzle-to-plate distances ($H/D < 4$) [4,29] links this occurrence with the interaction of the shear-layer vortices with the plate.

Comparing the curves of nozzle spacing $H/D = 2$ with those of $H/D = 5$, in the impingement region ($r/D < 2$), the Nusselt number values portray a general augmentation for the increased plate distance. Because the potential core length is in the order of 4–5D, the larger injection-to-plate spacing enables the penetration of the shear-layer turbulence toward the centerline axis, which results in a broad enhancement of heat transfer, including the impingement point. Furthermore, the two local maxima observed for $H/D = 2$, although much less pronounced and largely reduced in magnitude, are still apparent for $H/D = 5$. Although this is atypical for large nozzle-to-plate distances, their presence is likely associated with the relatively high jet velocity ($V_j = 65$ m/s, $Re = 34,000$) [37], which has an influence on the shear-layer vortex formation and its local heat transfer implications.

Analyzing the findings associated with the effectiveness distribution for the $H/D = 2$ spacing case (Fig. 9), η appears to be roughly uniform at a value of 1 throughout the entire impingement region ($r/D < 2$). Because the adiabatic wall temperature is nearly equal to the jet total temperature, the small difference may be associated with the slab recuperation factor. At $r/D = 1.6$, the slight

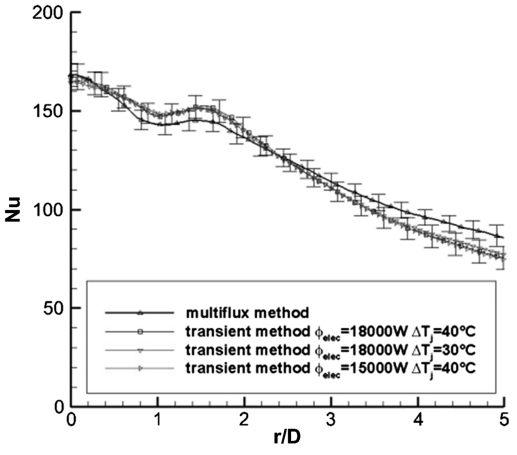

Fig. 6 Methodology comparison: Nusselt-number distribution over steel slab for $Re = 34,000$ and $H/D = 5$.

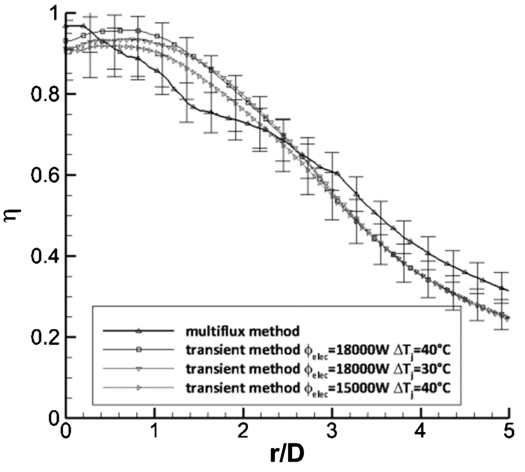

Fig. 7 Methodology comparison: effectiveness distribution over steel slab for $Re = 34,000$ and $H/D = 5$.

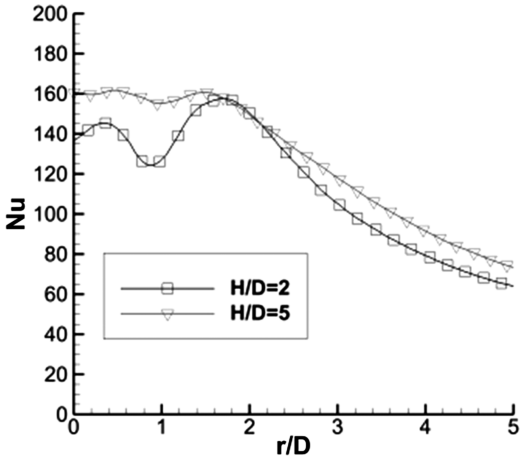

Fig. 8 Nusselt-number distribution over Inconel slab at $Re = 34{,}000$.

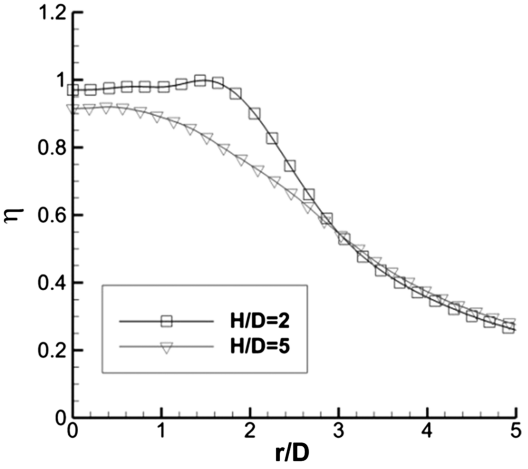

Fig. 9 Effectiveness distribution over Inconel slab at $Re = 34{,}000$.

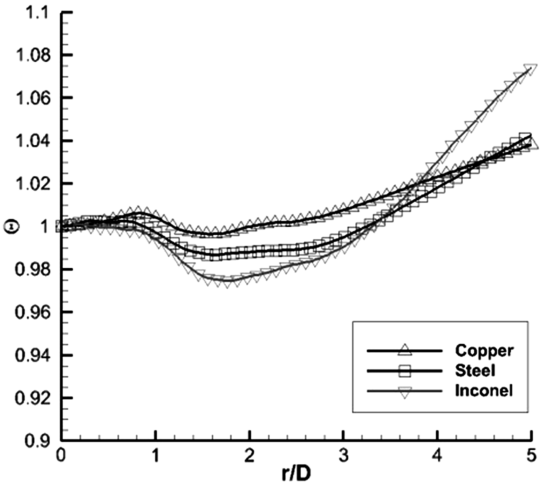

Fig. 10 Normalized temperature variation for $Re = 34{,}000$ and $H/D = 5$.

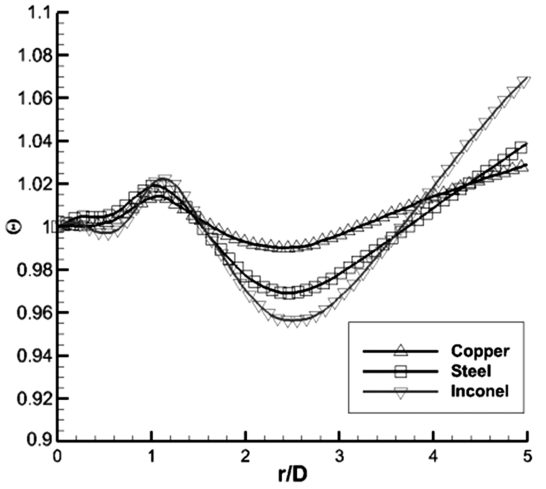

Fig. 11 Normalized temperature variation for $Re = 34{,}000$ and $H/D = 2$.

local effectiveness maximum is representative of high-velocity impinging jets, as prior recorded in [38]. In contrast, at the higher nozzle spacing of $H/D = 5$, η is found to be consistently less than 1, even at the impinging point. This is a consequence of postejection widening of the jet stream and the associated entrainment of the cooler surrounding fluid, which induces a drop in local jet temperature and hence in effectiveness. Similarly, at greater radial distances ($r/D > 1.6$), for both geometrical configurations, the effectiveness gradually decreases as a consequence of shear-layer vortex driven fresh air entrainment into the wall jet.

C. Local Effect of Conjugate Coupling

To determine the influence of conduction on the investigated configuration of jet impingement heat transfer, and hence assessing the significance of the conjugate effect, experiments were conducted for the three slab materials (copper, steel, Inconel) subjected to two different jet Reynolds numbers ($Re = 34,000$ and 37,000) at two distinct nozzle-to-plate spacings ($H/D = 2$ and 5).

1. Temperature Distributions

Figures 10 and 11 illustrate the nondimensional wall temperature for all three materials at two different geometric conditions $Re = 34,000$, $H/D = 5$ and $Re = 34,000$, $H/D = 2$, respectively. In both cases, the immediate vicinity of the impingement point exhibits a relatively flat temperature region, followed by a local maximum and a subsequent local drop in temperatures. At increased radial distances, with large changes in local temperature distributions, the reduction of the jet core's influence on local heat transfer coefficient is apparent. Contrasting the findings for different materials, the high thermal conductivity of copper promotes a significant reallocation of heat flux inside the slab, which entails a largely homogenous surface temperature; the maximum variation is less than 2.5 K ($\Delta\theta < 0.045$). In comparison with Inconel, which has the lowest thermal conductivity among the tested materials, the local wall temperature variation is up to 8 K ($\Delta\theta \sim 0.12$), predominantly located in the $r/D = 2.6$–4 region.

The temperature local maximum occurs at the same location for all materials and corresponds to the radial position of $r/D = 0.8$ for $H/D = 5$ (Fig. 10) and $r/D = 1$ for $H/D = 2$ (Fig. 11). This is the region that corresponds to a local drop in heat transfer that is driven by the nonuniform turbulence intensity of the jet impingement, as represented in Fig. 8, being more apparent at smaller nozzle to plate distances. As the flow turns radially outward to the wall jet region, the interaction of the shear-layer driven vortices with the plate causes a local temperature minimum at $r/D \sim 1.6$, followed by a gradual outward increase in surface temperature. The radial gradient, represented in Figs. 10 and 11 by the lower-temperature slopes observed for steel and Inconel plates, is inversely proportional to the slab thermal conductivity.

2. Heat Transfer Distributions

Complementing the surface temperature distributions, Figs. 12–17 chart the distributions of Nusselt number and effectiveness at two injection Reynolds numbers ($Re = 34,000$ and 37,000), for two nozzle-to-plate distances ($H/D = 2$ and 5). To evaluate conjugate heat transfer implications of the three slab materials (copper, steel, Inconel) in an impartial manner, the calculated Nusselt number

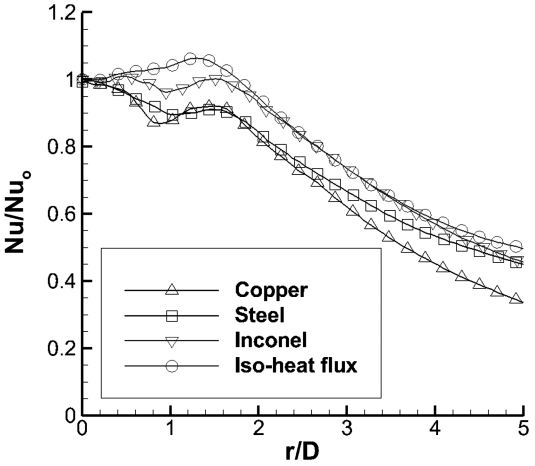

Fig. 12 Nusselt-number variation for $Re = 34{,}000$ and $H/D = 5$.

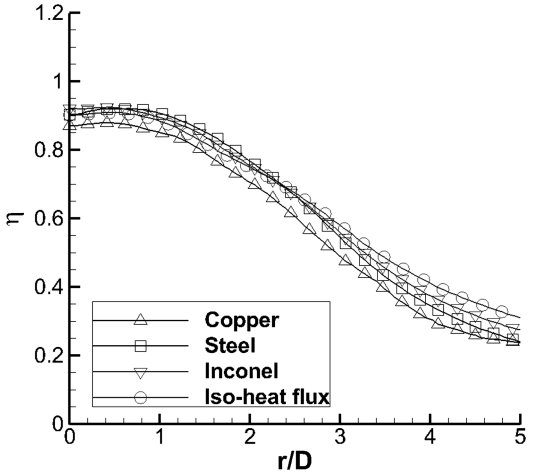

Fig. 13 Effectiveness variation for $Re = 34{,}000$ and $H/D = 5$.

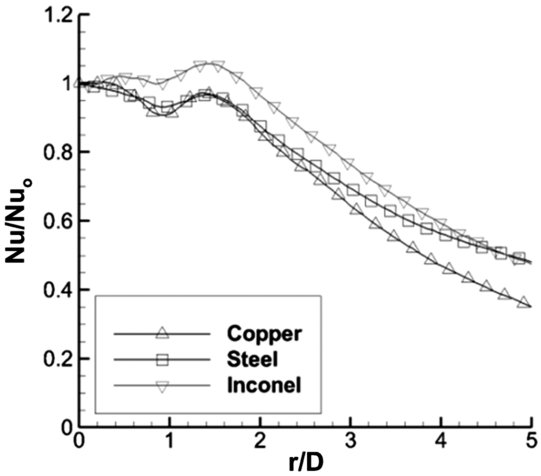

Fig. 14 Nusselt-number distribution for $Re = 37{,}000$ and $H/D = 5$.

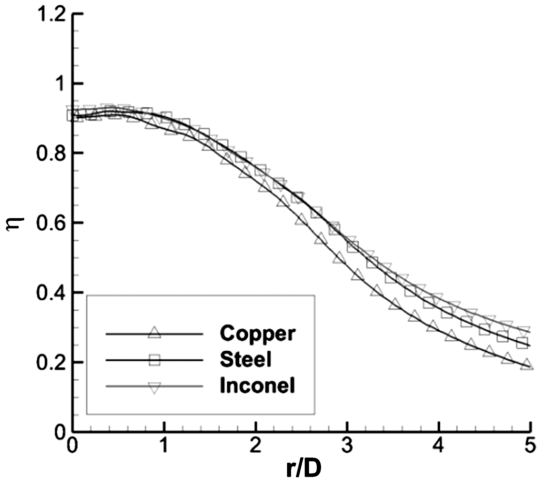

Fig. 15 Effectiveness distribution for $Re = 37{,}000$ and $H/D = 5$.

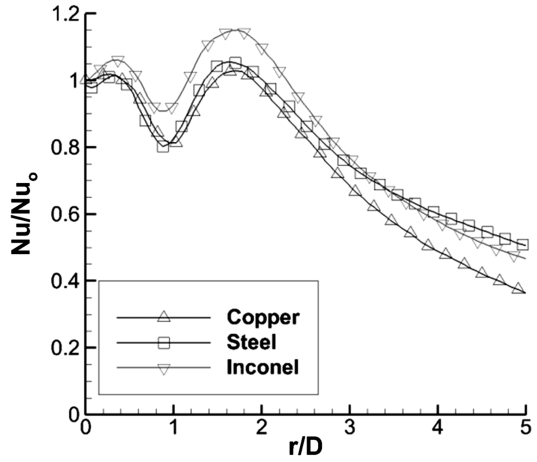

Fig. 16 Nusselt-number distribution for $Re = 34{,}000$ and $H/D = 2$.

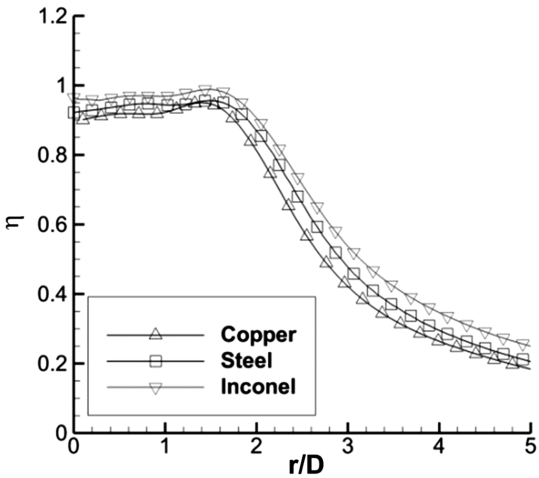

Fig. 17 Effectiveness distribution for $Re = 34{,}000$ and $H/D = 2$.

distribution was normalized with its respective value at the impingement point, which corresponds to the newly initializing boundary layer. Moreover, for the baseline configuration of $Re = 34,000$ and $H/D = 5$, an additional test case of isoheat-flux interface boundary condition was investigated. In contrast to the copper plate (with high conductivity and close to isothermal temperature distribution), where relatively large flux redistribution is inevitably present, the isoheat-flux boundary condition is analogous to the purely axial conduction within the slab.

As seen in Fig. 12, plate-material-dependent Nusselt number variations among the three slabs begin in the immediate vicinity of the symmetry axis ($r/D = 0$). For the copper and steel cases, the impingement point is associated with a maximum in normalized Nusselt number, which gradually decreases in the radial direction until a local minimum is reached at $r/D \sim 0.8$. The Inconel plate, however, exhibits a local minimum at the impingement point, followed by a maximum at $r/D = 0.3$ and a subsequent reduction at larger radial distances up to $r/D \sim 0.8$. For the isoheat-flux case, a monotonous increase in local Nusselt number is observed to span from the impingement point until $r/D \sim 1.4$. For the metal cases, the further outward local maximum at $r/D = 1.6$ appears more pronounced for Inconel, which is consistent with the dimensionless

wall temperature trends shown in Fig. 10. Similar observations can be made for the higher-Reynolds-number case ($Re = 37,000$), presented in Fig. 14. The findings suggest that the jet velocity profile and turbulence are not the only factors influencing the local heat transfer in the impingement zone and that the thermal boundary-layer development also has an effect.

In the wall jet region, for $r/D > 1.6$, the Nusselt number development decays monotonously for all cases (Fig. 12), where the difference in values associated with copper and Inconel plates is observed to remain mostly constant along the entire radial direction ($1.6 < r/D < 5$). However, the findings for the steel plate show no such correlation, and the Nusselt values up to a radial position of about $r/D = 2$ follow those of the copper plate, whereas at greater radial distances, the curve shifts toward the Inconel plate results. The findings are consistent with measurement configurations associated with higher Reynolds number and smaller jet-to-plate distance (Figs. 14 and 16, respectively).

This behavior can be explained by comparing the local temperature distributions (Fig. 10) with the local heat transfer coefficients (Fig. 12). For a surface temperature higher than the surrounding fluid, if the wall temperature increases in the flow direction (increasing temperature head), the lower layers of fluid at the adjoining wall come into contact with the increasingly hotter wall, yielding a local temperature increase within these layers. Consequently, the cross-sectional temperature gradients near the wall turn out to be greater than in the case of constant wall temperature, which leads to higher-than-isothermal surface heat transfer coefficients. This was previously discussed in the analytical conjugate heat transfer solution for laminar duct flows [13]. Hence, for the wall jet region at $r/D > 1.6$, the classification of high-to-low heat transfer configurations follow the sequence according to local radial temperature gradients (Inconel, steel, copper) and thereby is proportional to the inverse of plate conductivities. In general, it is apparent that, regardless of the given jet Reynolds number or nozzle-to-plate distance H/D (Figs. 12, 14, and 16), the normalized Nusselt number is lower for the copper plate than for the less conductive materials. Local variations can be as large as 20%, however; typically the differences are of the order of 8%. It is noteworthy that these values are significantly larger than the uncertainty level of 3.7%.

Considering that the copper slab represents a highly conductive surface (close to isothermal), the uniform flux at the boundary provides a second limit to the conjugate interaction (Fig. 12). For a low conjugate Nusselt region, the local energy input to the flow is higher for the isoheat-flux (convective) case because equal amounts of heat flux are imposed on the boundary layer independent of the local heat transfer coefficient. This could imply that, under these circumstances, the surface boundary layer will have a stronger gradient in the purely convective case than in the conjugate case, yielding higher heat transfer regions for the isoheat-flux boundary condition. As a consequence, all conjugate Nusselt number distributions lay within these two limits of isoheat-flux and isothermal boundary conditions.

Last, for all test cases, the effectiveness distributions along the radial distance are provided in Figs. 13, 15, and 17. The effectiveness values of the copper are found to be consistently lower than those of steel and Inconel, perhaps associated with the rapid radial decrease of Nusselt number. Because η represents the nondimensional fluid reference temperature linked to the fluid jet temperature, the decrease of heat transfer from the slab to the fluid implies a lower fluid temperature and hence effectiveness η. Nevertheless, deviations of η among the different materials (although systematic) are significantly smaller (almost one order of magnitude) than the respective uncertainties. Therefore, it is possible that the deviations are attributed to measurement errors.

D. Global Effect of Conduction on Convective Heat Transfer

Toward providing a more global perspective to the implications of conjugate jet impingement heat transfer, the Nusselt number distributions are spatially averaged ($0 < r/D < 5$) for all tested conditions (Table 2). Quantifiable differences in heat transfer are observed for different plate materials. Regardless of geometrical or aerodynamic conditions, the averaged Nusselt number values are consistently the lowest for the copper slab, whereas the highest values of $\bar{Nu}$ are attained for Inconel. This is consistent with analytical solutions for steady heat transfer to laminar flow in a circular duct, suggesting that the Nusselt numbers ensuing from a uniform temperature boundary condition provide a lower bound for conjugate cases [15]. The maximum averaged Nusselt number discrepancy detected between Inconel and copper can be up to 9%, as observed in the test case of $Re = 34,000$ at $H/D = 5$.

Table 2 Averaged values of Nusselt number

Material	$Re = 34,000$, $H/D = 5$	$Re = 37,000$, $H/D = 5$	$Re = 34,000$, $H/D = 2$
Copper	100	108	96
Steel	105	113	97
Inconel	109	116	99

Hence, in the scope of the present investigation, the adiabatic wall temperature reference is not sufficient to decouple conduction effects from convective heat transfer. Anderson [21] numerically demonstrated that the condition required for the validity of this assumption is $Bi > 1$, and the Biot number of the investigated cases varies between 0.007 and 0.02 for copper, 0.2 and 0.4 for steel, and 0.3 and 0.7 for Inconel.

V. Conclusions

In the scope of the current research, a new transient conjugate heat transfer measurement methodology was developed and validated against an established steady-state measurement technique, which has been adapted to the conjugate jet impingement problem. Based on a rapid change in jet temperature, the new methodology is shown to have a comparable level of Nusselt-number accuracy and improved effectiveness uncertainty, all while reducing the measurement duration and effort significantly.

An experimental investigation was conducted to measure and analyze the heat transfer due to an air jet impingement on a plate while explicitly taking into account the conduction inside the solid. Three plate materials (copper, steel, and Inconel) with different thermal conductivities were chosen for assessing the significance of the conjugate effect on the resulting profiles of heat transfer enhancement. The conjugate heat transfer findings indicated that, by changing the impingement plate material, the average heat transfer is observed to vary by up to 9%, regardless of the injection Reynolds number or nozzle-to-plate distance H/D. Averaged Nusselt number values were consistently low for a copper plate, whereas the highest values were obtained for Inconel. Local Nusselt-number distributions indicate variations between the copper and Inconel plate of up to 20%; however, typical variations were in the order of 8%. Comparing the findings with the purely convective benchmark, it was observed that isoheat-flux boundary condition yields a Nusselt number upper bound, and the isothermal interface boundary condition constitutes a lower bound on all conjugate distributions.

In general, although the measured deviations in Nusselt number among the plate materials can be considered relatively small, neglecting the conjugate effect can amount to significant errors in wall temperature prediction, particularly in the presence of high heat-flux levels.

References

[1] Martin, H., "Heat and Mass Transfer Between Impinging Gas Jets and Solid Surfaces," *Advances in Heat Transfer*, Vol. 4, 1977, pp. 1–60. doi:10.1016/S0065-2717(08)70221-1

[2] Jambunathan, K., Lai, E., Moss, M. A., and Button, B. L., "A Review of Heat Transfer Data for Single Circular Jet Impingement," *International Journal of Heat and Fluid Flow*, Vol. 13, No. 2, June 1992, pp. 106–115. doi:10.1016/0142-727X(92)90017-4

[3] Zuckerman, N., and Lior, N., "Jet Impingement Heat Transfer: Physics, Correlations, and Numerical Modeling," *Advances in Heat Transfer*,

Vol. 39, 2006, pp. 565–631.
doi:10.1016/S0065-2717(06)39006-5

[4] Baughn, J. W., and Shimizu, S., "Heat Transfer Measurements from a Surface with Uniform Heat Flux and an Impinging Jet," *Journal of Heat Transfer*, Vol. 111, No. 4, 1989, pp. 1096–1098.
doi:10.1115/1.3250776

[5] Fénot, M., Vullierme, J.-J., and Dorignac, E., "A Heat Transfer Measurement of Jet Impingement with High Injection Temperature," *Comptes Rendus Mécanique*, Vol. 333, No. 10, 2005, pp. 778–782.
doi:10.1016/j.crme.2005.08.002

[6] Sagot, B., Antonini, G., Christgen, A., and Buron, F., "Jet Impingement Heat Transfer on a Flat Plate at a Constant Wall Temperature," *International Journal of Thermal Sciences*, Vol. 47, No. 12, 2008, pp. 1610–1619.
doi:10.1016/j.ijthermalsci.2007.10.020

[7] von Wolfersdorf, J., Hoecker, R., and Sattelmayer, T., "A Hybrid Transient Step-Heating Heat Transfer Measurement Technique Using Heater Foils and Liquid-Crystal Thermography," *Journal of Heat Transfer*, Vol. 115, No. 2, 1993, pp. 319–324.
doi:10.1115/1.2910682

[8] Luikov, A. V., "Conjugate Heat Transfer Problems," *International Journal of Heat and Mass Transfer*, Vol. 17, No. 2, 1974, pp. 257–265.
doi:10.1016/0017-9310(74)90087-8

[9] Cole, K. D., "Conjugate Heat Transfer from a Small Heated Strip," *International Journal of Heat and Mass Transfer*, Vol. 40, No. 11, 1997, pp. 2709–2719.
doi:10.1016/S0017-9310(96)00232-3

[10] Perelman, T., "On Conjugated Problems of Heat Transfer," *International Journal of Heat and Mass Transfer*, Vol. 3, No. 4, 1961, pp. 293–303.
doi:10.1016/0017-9310(61)90044-8

[11] Dorfman, A. S., *Heat Transfer for Flows Past Non-Isothermal Bodies*, Izdatel'stvo Mashinostroenie, Moscow, 1982, p. 192.

[12] Dorfman, A. S., "A New Type of Boundary Condition in Convective Heat Transfer Problems," *International Journal of Heat and Mass Transfer*, Vol. 28, No. 6, 1985, pp. 1197–1203.
doi:10.1016/0017-9310(85)90127-9

[13] Dorfman, A., and Renner, Z., "Conjugate Problems in Convective Heat Transfer: Review," *Mathematical Problems in Engineering*, Vol. 2009, 2009, p. 27, Article ID 927350.
doi:10.1155/2009/927350

[14] Dorfman, A., *Exact Solution of Thermal Boundary Layer Equation with Arbitrary Temperature Distribution on Streamlined Surface*, High Temp 8, No. 5, 1971, pp. 955–963.

[15] Mori, S., Sakakibara, M., and Tanimoto, A., "Steady Heat Transfer to Laminar Flow in a Circular Tube with Conduction in the Tube Wall," *Heat Transfer Japanese Research*, Vol. 3, 1974, pp. 37–46.

[16] Barozzi, G. S., and Pagliarini, G., "A Method to Solve Conjugate Heat Transfer Problems: The Case of Fully Developed Laminar Flow in a Pipe," *Journal of Heat Transfer*, Vol. 107, No. 1, 1985, pp. 77–83.
doi:10.1115/1.3247406

[17] Luikov, A. V., Aleksachenko, V. A., and Aleksachenko, A. A., "Analytical Methods of Solution of Conjugate Problems in Convective Heat Transfer," *International Journal of Heat and Mass Transfer*, Vol. 14, No. 8, 1971, pp. 1047–1056.
doi:10.1016/0017-9310(71)90203-1

[18] Pozzi, A., Quaranta, G., and Tognaccini, R., "A Self-Similar Unsteady Flow with Conjugated Heat Transfer," *International Journal of Heat and Mass Transfer*, Vol. 51, Nos. 7–8, 2008, pp. 1804–1809.
doi:10.1016/j.ijheatmasstransfer.2007.07.003

[19] Mosaad, M., "Laminar Forced Convection Conjugate Heat Transfer over a Flat Plate," *Heat and Mass Transfer*, Vol. 35, No. 5, 1999, pp. 371–375.
doi:10.1007/s002310050338

[20] Azar, K., and Moffat, R. J., "Evaluation of Different Heat Transfer Coefficient Definitions," *Electronics Cooling* (online journal), June 1995, http://www.electronics-cooling.com/1995/06/evaluation-of-different-heat-transfer-coefficient-definitions/.

[21] Anderson, A. M., "Decoupling Convective and Conductive Heat Transfer Using the Adiabatic Heat Transfer Coefficient," *Journal of Electronic Packaging*, Vol. 116, No. 4, 1994, pp. 310–316.
doi:10.1115/1.2905703

[22] Rahman, M. M., Bula, A. J., and Leland, J. E., "Analysis of Transient Conjugate Heat Transfer to a Free Impinging Jet," *Journal of Thermophysics and Heat Transfer*, Vol. 14, No. 3, 2000, pp. 330–339.
doi:10.2514/2.6549

[23] Wang, X. S., Dagan, Z., and Jiji, L. M., "Heat Transfer Between a Circular Free Impinging Jet and a Solid Surface with Non-Uniform Wall Temperature or Wall Heat Flux—1. Solution for the Stagnation Region," *International Journal of Heat and Mass Transfer*, Vol. 32, No. 7, 1989, pp. 1351–1360.
doi:10.1016/0017-9310(89)90034-3

[24] Wang, X. S., Dagan, Z., and Jiji, L. M., "Heat Transfer Between a Circular Free Impinging Jet and a Solid Surface with Non-Uniform Wall Temperature or Wall Heat Flux—2. Solution for the Boundary Layer Region," *International Journal of Heat and Mass Transfer*, Vol. 32, No. 7, 1989, pp. 1361–1371.
doi:10.1016/0017-9310(89)90035-5

[25] Ireland, P. T., Neely, A. J., and Gillespie, D. R. H., "Turbulent Heat Transfer Measurements Using Liquid Crystals," *International Journal of Heat and Fluid Flow*, Vol. 20, No. 4, 1999, pp. 355–367.
doi:10.1016/S0142-727X(99)00030-2

[26] Spring, S., Xing, Y., and Weigand, B., "An Experimental and Numerical Study of Heat Transfer from Arrays of Impinging Jets with Surface Ribs," *Journal of Heat Transfer*, Vol. 134, No. 8, 2012, Paper 082201.
doi:10.1115/1.4006155

[27] Ortega, A., and Ramanathan, S., "On the Use of Point Source Solutions for Forced Air Cooling of Electronic Components—Part 2: Conjugate Forced Convection from a Discrete Rectangular Source on a Thin Conducting Plate," *Journal of Electronic Packaging*, Vol. 125, No. 2, 2003, pp. 235–243.
doi:10.1115/1.1569507

[28] Cukurel, B., Selcan, C., and Arts, T., "Film Cooling Extraction Effects on the Aero-Thermal Characteristics of Rib Roughened Cooling Channel Flow," *ASME Journal of Turbomachinery*, Vol. 135, No. 2, 2012, pp. 021016-1–021016-12.
doi:10.1115/1.4007501.

[29] Fénot, M., Vullierme, J.-J., and Dorignac, E., "Local Heat Transfer due to Several Configurations of Circular Air Jets Impinging on a Flat Plate with and Without Semi-Confinement," *International Journal of Thermal Sciences*, Vol. 44, No. 7, 2005, pp. 665–675.
doi:10.1016/j.ijthermalsci.2004.12.002

[30] Goldstein, R. J., Sobolik, K. A., and Seol, W. S., "Effect of Entrainment on the Heat Transfer to a Heated Circular Air Jet Impinging on a Flat Surface," *Journal of Heat Transfer*, Vol. 112, No. 3, 1990, pp. 608–611.
doi:10.1115/1.2910430

[31] Kline, S. J., and McClintock, F. A., "Describing Uncertainties in Single-Sample Experiments," *Mechanical Engineering*, Vol. 75, No. 1, 1953, pp. 3–8.

[32] Rabin, Y., "A General Model for the Propagation of Uncertainty in Measurements into Heat Transfer Simulations and its Application to Cryosurgery," *Cryobiology*, Vol. 46, No. 2, 2003, pp. 109–120.
doi:10.1016/S0011-2240(03)00015-4

[33] Hofmann, H. M., Kaisera, R., Kinda, M., and Martina, H., "Calculations of Steady and Pulsating Impinging Jets—An Assessment of 13 Widely Used Turbulence Models," *Numerical Heat Transfer, Part B: Fundamentals*, Vol. 51, No. 6, 2007, pp. 565–583.
doi:10.1080/10407790701227328

[34] Lee, J., and Lee, S.-J., "The Effect of Nozzle Configuration on Stagnation Region Heat Transfer Enhancement of Axisymmetric Jet Impingement," *International Journal of Heat and Mass Transfer*, Vol. 43, No. 18, 2000, pp. 3497–3509.
doi:10.1016/S0017-9310(99)00349-X

[35] Lytle, D., and Webb, B. W., "Air Jet Impingement Heat Transfer at Low Nozzle-Plate Spacings," *International Journal of Heat and Mass Transfer*, Vol. 37, No. 12, 1994, pp. 1687–1697.
doi:10.1016/0017-9310(94)90059-0

[36] Roux, S., Fénot, M., Lalizel, G., Brizzi, L.-E., and Dorignac, E., "Experimental Investigation of the Flow and Heat Transfer of an Impinging Jet Under Acoustic Excitation," *International Journal of Heat and Mass Transfer*, Vol. 54, Nos. 15–16, 2011, pp. 3277–3290.
doi:10.1016/j.ijheatmasstransfer.2011.03.059

[37] Limaye, M. D., Vedula, R. P., and Prabhu, S. V., "Local Heat Transfer Distribution on a Flat Plate Impinged by a Compressible Round Air Jet," *International Journal of Thermal Sciences*, Vol. 49, No. 11, 2010, pp. 2157–2168.
doi:10.1016/j.ijthermalsci.2010.06.020

[38] Brevet, P., Dorignac, E., and Vullierme, J. J., "Mach Number Effect on Jet Impingement Heat Transfer," *Annals of New York Academics of Sciences*, Vol. 934, May 2001, pp. 409–416.
doi:10.1111/j.1749-6632.2001.tb05877.x